

A+D-Net: Shadow Detection with Adversarial Shadow Attenuation

Hieu Le, Tomas F. Yago Vicente, Vu Nguyen, Minh Hoai, Dimitris Samaras
Stony Brook University, Stony Brook, NY 11794, USA

{hle, tyagovicente, vhnghuyen, minhhoai, samaras}@cs.stonybrook.edu

Abstract

Single image shadow detection is a very challenging problem because of the limited amount of information available in one image, as well as the scarcity of annotated training data. In this work, we propose a novel adversarial training based framework that yields a high performance shadow detection network (D-Net). D-Net is trained together with an Attenuator network (A-Net) that generates adversarial training examples. A-Net performs shadow attenuation in original training images constrained by a simplified physical shadow model and focused on fooling D-Net’s shadow predictions. Hence, it is effectively augmenting the training data for D-Net with hard to predict cases. Experimental results on the most challenging shadow detection benchmark[22] show that our method outperform the state-of-the-art[14] with a 38% error reduction, measured in terms of balanced error rate (BER). Our proposed shadow detector also obtains state-of-the-art results on a cross-dataset task testing on UCF[24] with a 14% error reduction. Furthermore, the proposed method can perform accurate close to real-time shadow detection at a rate of 13 frames per second.

1. Introduction

Shadow detection is an important problem in computer vision. Shadows occur frequently in natural scenes, and the presence of shadows hampers many tasks such image segmentation, object tracking, and semantic labeling. Shadows are formed due to the complex physical interactions between the light sources and the geometry and materials of the objects present in a scene. Knowing information about the physical environment such as the sparse 3D reconstruction of the scene[23], rough geometry estimates[15], and multiple images of the same scene under different illumination conditions[19] can aid shadow detection. Unfortunately, the amount of information captured by a single image of the scene is limited, and inferring the physical structure of a general scene from a single image is still a difficult problem by itself.

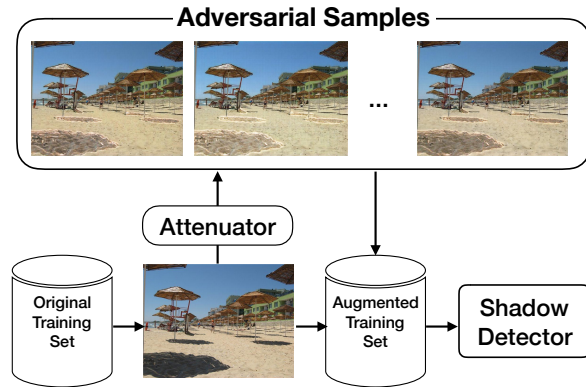


Figure 1: **Adversarial shadow attenuation.** The attenuator takes an original shadow image and generates different adversarial shadow samples to train the shadow detector.

The difficulty of shadow detection is exacerbated when dealing with consumer-grade photographs and web images [11]. These types of images often come from non-linear camera sensors, containing many compression and noise artifacts. In this context, it is more appropriate to model the appearance of shadows from data [4, 9, 20, 24] rather than rely on physical models of illumination[1, 2].

While nowadays we have powerful classification models such as deep neural networks, they must be trained with a large amount of annotated data. Unfortunately, annotated shadow data is expensive to collect and label. It has not been until recently that available training data has moved from a few hundred images [4, 24] to a few thousands [22]. Automatic removal of shadows in a single image, which is very related to shadow detection, is even more challenging. There is little training data to learn the mapping from shadow to shadow-free images. Furthermore, the existing available shadow and shadow-free image pairs come from a very limited space of scenes. These images come from a setup where the camera is in a fixed position. Then, either the occluder object casting the shadow is out of the camera field of view and can be removed (see Figure 2 second row), or it is an outdoors scene captured over time as the

shadows cast by the sun vary in location based on the time of the day (see Figure 2 first row). This does not approximate well the wide variety of images of natural scenes that contain shadows.

In this work, we propose to leverage the limited existing shadow annotated data (shadow image plus corresponding shadow mask) to learn a shadow attenuation network (A-Net). This network modifies original shadow images so as to weaken the shadow effect, see Figure 1. These generated images, serve as additional challenging training samples for a shadow detector (D-Net). We present a novel framework, where the shadow attenuator and the shadow detector are trained jointly in an adversarial manner. The output of the attenuation model A-Net provides training samples with harder to detect shadow areas improving the overall reliability of the detector D-Net. Experimental results show that our proposed shadow detector achieves outstanding performance in the most challenging shadow detection benchmark SBU [22]: measured in terms of Balanced Error Rate (BER), we obtain a 38% error reduction compared to the state of the art method [14]. Furthermore, on the cross-dataset task (training and testing on different datasets), our method reduces the testing error in UCF [24] by 14% compared to the state of the art [14].

We designed our training scheme so as to enforce A-Net to only modify the shadow areas of the input image, while further constraining A-Net’s edits to follow a physical model of illumination. Moreover, in the absence of a stronger training signal, A-Net hallucinates intensity/color corrections to attenuate the shadow areas so as to fool D-Net. In this manner, although A-Net produces realistic results, we are not tackling single image shadow removal. It would be too ambitious of a goal since our framework does not learn from actual shadow removal data (pairs of shadow/shadow-free images). This work contains the following contributions:

- A novel adversarial framework to train a shadow detector that outperforms the state-of-the-art by a wide margin.
- We are, to the best of our knowledge, first to use generated adversarial examples to improve shadow detection.
- The proposed method is, to the best of our knowledge, the first accurate shadow detector that performs close to real time (13fps).

2. Related Work

Single image shadow detection is a well studied problem. Earlier work, focused on physical modeling of illumination [1, 2]. These methods render illumination invariant representations of the images where shadow de-

tection is trivial. These methods, however, only work well for high quality images taken with narrow-band sensors [11]. For general images, data-driven approaches based on learning classifiers [5, 7, 9, 20] from small annotated datasets [4, 24] have shown more success. For instance, Vicente *et al.* [20] optimized a multi-kernel Least-Squares SVM based on leave-one-out estimates. This approach yielded very accurate results on UCF [24] and UIUC [4] datasets. However, the method does not scale well to handle larger amount of training data, like the recently released SBU shadow dataset [22].



Figure 2: **Shadow/shadow-free data examples.** Examples of corresponding shadow and shadow-free image pairs from SRD shadow removal dataset [16].

The SBU dataset contains 4K training images. It is worth noting that the accompanying shadow training masks come from weak annotations [21]. A stacked-CNN architecture that refines the predictions of an image-level FCN with a patch-CNN was proposed by [22] to properly profit from a larger amount of training data. This approach achieves good detection results on the challenging SBU test set [22], as well as on the cross-dataset task testing on UCF [24]. However, this method is cumbersome as the Fully Connected Network (FCN) has to be trained first and then its predictions used to train the patch-CNN. Similarly, testing is computationally expensive as it requires the FCN prediction followed by predictions of densely sampled patches covering the testing image. Most recently, Nguyen *et al.* [14] presented scGAN, a method based on Generative Adversarial Networks (GANs) [3]. They proposed a parametric conditional GAN [12] framework, where the generator is conditioned on input RGB images and learns to generate the corresponding shadow mask. To detect shadows in a given image, they combine the prediction masks for a large quantity of multi-scale crops. In this manner they obtain state of the art results on SBU, however, testing is computationally expensive.

Our proposed adversarial framework is related to the recently proposed Simulated+Unsupervised approach by Shrivastava *et al.* [18]. In this work they adversarially trained a Refiner network that takes as input synthetic ex-

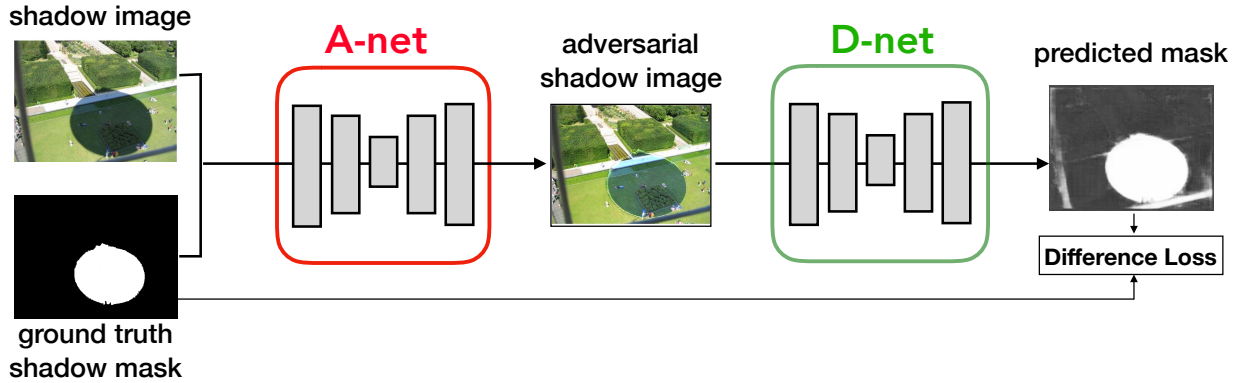


Figure 3: **Adversarial framework diagram.** A-Net takes a shadow image and its corresponding shadow mask as input, and generates an adversarial example by attenuating the shadows present on the input image. The generated image contains a less discernible shadow area, hence harder to detect. D-Net takes this image as input and aims to recover the original shadow mask.

amples and makes them look realistic. The refined examples can be used as additional training data. In a similar way, our proposed Attenuator (A-Net) takes original training images and generates realistic images with attenuated shadows that act as additional training examples for our shadow detector. The generation of adversarial examples is an integral part of the joint training process with the detector (D-Net), in contrast to [18] where the generated data is a preprocessing step to enrich the training set. The effects of the shadow Attenuator can also be seen as related to adversarial perturbations[13]: A-Net modifies the input images so as to fool the predictions of the shadow detector D-Net.

3. Proposed Shadow Detection Framework

We present a novel framework for shadow detection based on adversarial training and shadow attenuation. Our proposed model contains two deep networks that are jointly trained. In Figure 3, we illustrate the flow diagram of our framework. The shadow attenuation network (called Attenuator or A-Net) takes as input a shadow image and its corresponding shadow mask. Based on these inputs, the Attenuator generates a version of the input image where the shadows have been attenuated. Attenuation can be thought of as partial shadow removal. The image generated by the Attenuator is then fed into a shadow detection network (called Detector or D-Net), which predicts the shadow areas from the generated image with attenuated shadows. On each training iteration, D-Net also takes the original input image (shadow training example), and learns to predict its corresponding shadow mask based on the annotated ground-truth mask.

The proposed A-Net learns to attenuate shadow regions to fool the shadow detector. In particular, for pixels inside

the provided shadow mask, A-Net manipulates the values of the pixels to disguise them as non-shadow pixels so that they cannot be recognized by D-Net. We further constrain the attenuation transformation using a loss that incorporates physics-inspired shadow domain knowledge. In this manner, we enhance the quality of the generated pixels. At the same time, A-Net learns not to change the values or the pixels outside the shadow mask. We enforce this with a loss that penalizes the difference between the generated image and the input image on the area outside of the shadow mask (non-shadow pixels). The adversarial training process with all the aforementioned constraints and the back propagation error from the shadow detection network guides A-Net to perform shadow attenuation.

The detector network, D-Net, takes the adversarial examples generated by A-Net and predicts a shadow mask. The shadow area in the image examples generated by A-Net is generally harder to detect than the input images. After all, A-Net is trained to attenuate the shadows to fool D-Net. As a result, D-Net is trained with challenging examples in addition to the original training examples. As D-Net improves its ability to detect shadows, A-Net must also improve its ability to attenuate shadows to confound D-Net with tougher adversarial examples. This process strengthens the shadow detection ability of D-Net.

Our framework can be interpreted as an adaptation of the GAN approach to the shadow domain, focusing on the pixel level. In this sense, the output of the proposed D-Net corresponds to real/fake decision at the pixel level, hence generating a segmentation map as a result. The proposed A-Net tries to fool D-Net by manipulating each shadow pixel.

In the following subsections, we describe the details of the structure, training process, and objectives of A-Net and D-Net.

3.1. Network Architectures

Both A-Net and D-Net are developed based on the U-Net architecture [17]. Following [8], we create networks with four skip-connection modules, each of which contains a sequence of Convolution, Batch Normalization, and Leaky-ReLu [6] layers. The input to an A-Net is a four channel image, which is the concatenation of the RGB image and the corresponding shadow mask. The output of A-Net is a three channel RGB image. The input to D-Net is an RGB image, and the output is a single channel shadow mask.

3.2. A-Net: Shadow Attenuator Network

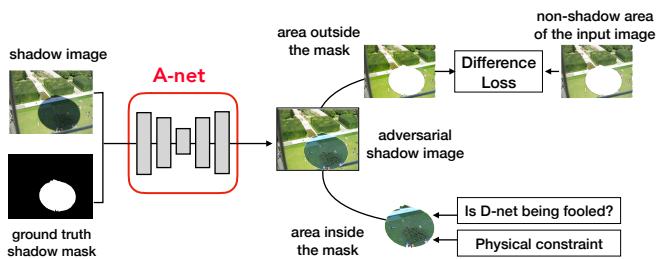


Figure 4: **A-Net configuration.** The area outside the shadow mask is constrained by the difference loss with respect to the input image. The area inside the shadow mask is constrained by the feedback from D-Net and the physics based constraint.

The shadow attenuator network A-Net is trained to re-illuminate only the shadow areas in an image so that these areas cannot be detected by the adversarial shadow detector network D-Net. To perform shadow attenuation properly, A-Net aims to fool D while not deviating from the physics model of shadow appearance. In Figure 4, we depict the training process of A-Net. A-Net seeks to attenuate shadow areas under the following constraints and objectives:

1. The values of non-shadow pixels from the input image are preserved.
2. The shadow pixels from the input image are re-illuminated such that D-Net cannot recognize them as shadow pixels.
3. The attenuation transformation results on the generated image obey a physics-inspired shadow constraint.

These constraints and objectives can be incorporated in the training of A-Net by defining a proper loss function. Let x denote an input image, and $M(x)$ be the shadow mask of x . Let $A(x)$ denote the output of A-Net for the input pair of x and $M(x)$ (here we write $A(x)$ as the short form for $A(x, M(x))$). Let $D(x)$ denote the output of D-Net for

an input image x . The objective of A-Net’s training is to minimize a weighted combination of three losses:

$$\mathcal{L}_A(x) = \lambda_{nsd}\mathcal{L}_{nsd}(x) + \lambda_{sd}\mathcal{L}_{sd}(x) + \lambda_{ph}\mathcal{L}_{ph}(x).$$

Where \mathcal{L}_{nsd} is the loss that penalizes the modification of values for pixels outside the shadow mask $M(x)$ for the input image x :

$$\mathcal{L}_{nsd}(x) = \text{mean}_{i \notin M(x)} \|A(x)_i - x_i\|_1. \quad (1)$$

\mathcal{L}_{sd} is the adversarial loss. It penalizes the correct recognition of D-Net for shadow pixels on the generated image, restricted to the area inside the training shadow mask $M(x)$:

$$\mathcal{L}_{sd}(x) = \text{mean}_{i \in M(x)} D(A(x))_i. \quad (2)$$

\mathcal{L}_{ph} is a physics inspired loss to ensure that the shadow area in the generated image is re-illuminated in a realistic manner. In this work, we use a simplified illumination model that was also used in [4, 5]. Let I be an image and I_i denote the i^{th} pixel of the image. Based on the illumination model, each pixel is lit as follows:

$$I_i = (k_i L_d + L_e) R_i,$$

where R_i is the surface reflectance corresponding to the i^{th} pixel. L_d and L_e are RGB vectors representing the direct light and the environment light (which models inter reflections), respectively. $k_i \in [0, 1]$ is the shadowing factor that indicates how much of the direct light reaches the pixel i . k_i remains close to 0 for the umbra region of the shadow, while it gets increasingly close to 1 in the penumbra region. For pixels within shadow-free areas $k_i = 1$ by default. We can relate the original shadow region and its corresponding shadow-free version by the ratio:

$$\frac{I_i^{\text{shadow-free}}}{I_i^{\text{shadow}}} = \frac{L_d + L_e}{k_i L_d + L_e}. \quad (3)$$

By taking the ratio between the shadow-free and shadow values, we have eliminated the unknown reflectance factor. We assume that the direct light is consistent over the scene depicted by the image, and that for each given pixel location the effects of the environment light are similar. Based on this model, we enforce that the per pixel ratio between the input image and the shadow attenuated image should not vary significantly. Working in the log RGB space, Equation (3) becomes the difference between A-Net’s output and the input image, and the loss is formalized as:

$$\mathcal{L}_{ph}(x) = \sum_{c \in \{R, G, B\}} \text{Variance}_{i \in M(x)} [\log(A(x)_i^c) - \log(x_i^c)].$$

where $(\cdot)^c$ denotes the pixel value in the channel c .

In Figure 5, we show examples of adversarial examples with attenuated shadows that are generated by A-Net along the training process.

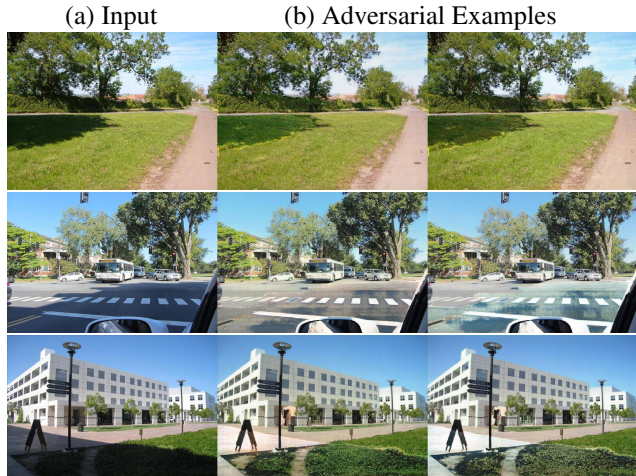


Figure 5: **Examples of attenuated shadows.** (a) Input image. (b) Adversarial examples with attenuated shadows generated by A-Net.

3.3. D-Net: Shadow Detector Network

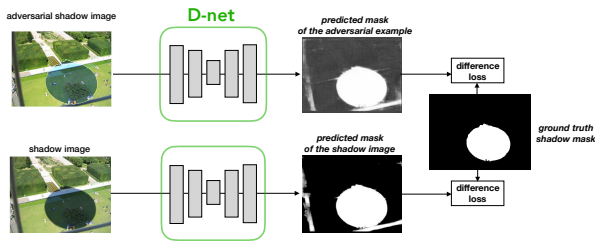


Figure 6: **D-Net configuration.** D-Net learns to detect shadows from both adversarial examples generated by A-net as well as original training examples.

D-Net plays the central role in our framework. D-Net learns to detect shadows from adversarial examples generated by A-Net as well as original training examples. On each training iteration, we feed both the input image and the adversarial example to D-Net and train D-Net to predict the ground-truth shadow mask. In Figure 6, we illustrate this process. The learning objective for D-Net is to minimize the following loss function:

$$\mathcal{L}_D(x) = \lambda_{real} \|D(x) - M(x)\|_1 + \lambda_{adversarial} \|D(A(x)) - M(x)\|_1, \quad (4)$$

where λ_{real} and $\lambda_{adversarial}$ are the two parameters controlling how much D-Net learns from the original and adversarial examples, respectively.

4. Experiments and Results

We perform experiments on several publicly available shadow datasets. One of them is the SBU Shadow dataset [22]. This dataset consists of pairs of RGB images and corresponding annotated shadow binary masks. The SBU dataset contains 4089 training images, and 638 testing images. This is currently the largest and most challenging available shadow benchmark. We also perform cross-dataset experiments on the UCF testing set [24], which contains 111 images with corresponding shadow masks. We quantitatively evaluate shadow detection performance by comparing the testing ground-truth shadow masks with the prediction masks produced by D-Net. As is common practice in the shadow detection literature, we will use the Balance Error Rate (BER) as the principal evaluation metric. BER is defined as:

$$BER = 1 - \frac{1}{2} \left(\frac{TP}{TP + FN} + \frac{TN}{TN + FP} \right) \quad (5)$$

where TP, TN, FP, FN are the total numbers of true positive, true negative, false positive, and false negative pixels respectively. Since natural images tend to contain an overwhelming majority of non-shadow pixels, BER is less biased than the mean pixel accuracy. For completeness, we also provide separate mean pixel error rates for shadow and non-shadow classes.

Training and implementation details. We use gradient descent with the Adam solver [10] to train our model. We use minibatch SGD with batch size of 32. On each training iteration, we perform three forward passes consecutively: forward the input shadow image to A-Net to get the adversarial example $A(x)$, then separately forward the adversarial image and shadow input image to D-Net. We alternate one parameter update step on D-Net with one update step on A-Net, as suggested by [3]. Before training and testing, we transform the images into log-space. We experimentally set our training parameters as: $(\lambda_{nsd}, \lambda_{sd}, \lambda_{ph}, \lambda_{real}, \lambda_{adversarial}) := (0.4, 0.2, 0.4, 0.8, 0.2)$. We implemented our framework on PyTorch. The code will be publicly available upon publication.

4.1. Evaluation of Shadow Detection

We evaluate the shadow detection performance of the proposed D-Net on the SBU dataset. In order to generate the shadow detection results, we first resize the input image into 256×256 . We feed-forward this image to D-net to produce a shadow mask of size 256×256 . Then, we resize the

Methods	BER	Shadow	Non Shad.
Stacked-CNN [22]	11.0	9.6	12.5
scGAN [14]	9.1	7.8	10.4
D-Net (this work)	5.7	6.2	5.2

Table 1: **Evaluation of shadow detection methods on the SBU Shadow dataset [22].** All methods are trained on the SBU training data, and tested on the SBU test data. Both Balance Error Rate (BER) and per class error rates are shown. Our proposed method achieves around 38% error reduction across metrics with respect to the state-of-the-art scGAN [14]. Best results printed in bold.

Method	BER	Shadow	Non Shad.
stacked-CNN [22]	13.0	9.0	17.1
scGAN [14]	11.5	7.7	15.3
D-Net (this work)	9.9	7.3	12.5

Table 2: **Comparison of shadow detection results for cross-dataset task.** All methods are trained on the SBU Train dataset [22] and evaluated on the UCF test set [24]. Our proposed method outperforms the previous state-of-the-art scGAN[14] by 14% in terms of balance error rate.

resulting mask back to the original size of the input image, and compare it to the provided ground-truth mask.

In Table 1, we compare our results with the state-of-the-art methods Stacked-CNN [22] and scGAN [14]. All methods are trained on the SBU training set. Performance on the SBU test set is reported in terms of BER, as well as shadow and non-shadow error rates. As can be seen, our detector (D-Net) outperforms the previous state-of-the-art methods by a wide margin. Compared to Stacked-CNN we obtain a 48% error reduction. With respect to the top performer scGAN, D-Net brings a 38% error reduction. D-Net also yields the lowest per class error rates for both shadow and non-shadow pixels.

We also perform challenging cross-dataset experiments as follows. We train a detector on the SBU dataset, and subsequently evaluate its performance on the test set of the UCF dataset [24]. These datasets are disjoint; while SBU covers a wide range of scenes, UCF focuses on images where dark shadows as well dark albedo objects are present. We report results for the cross-dataset task in Table 2. Again, we compare our method with the previous state-of-the-art methods: Stacked-CNN [22] and scGAN [14]. In terms of BER, our proposed D-Net yields significant error reductions of 24% and 14% with respect to Stacked-CNN and scGAN, respectively. In this experiment, our proposed method also achieves the lowest per class error rates for both shadow and non-shadow areas.

4.2. Qualitative Results

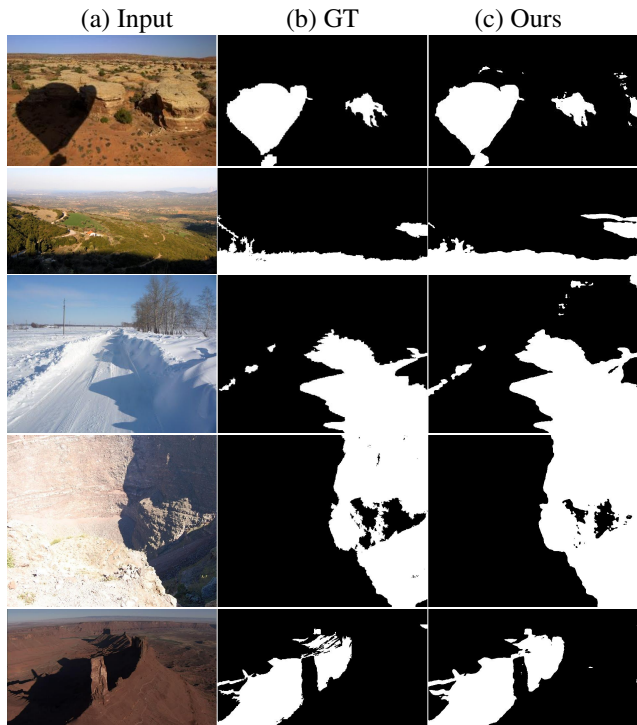


Figure 7: **Shadow detection examples.** Our proposed method correctly detects shadows on different scenes, and illumination conditions. (a) Input image. (b) Ground-truth shadow mask. (c) Predicted shadow mask by our method.

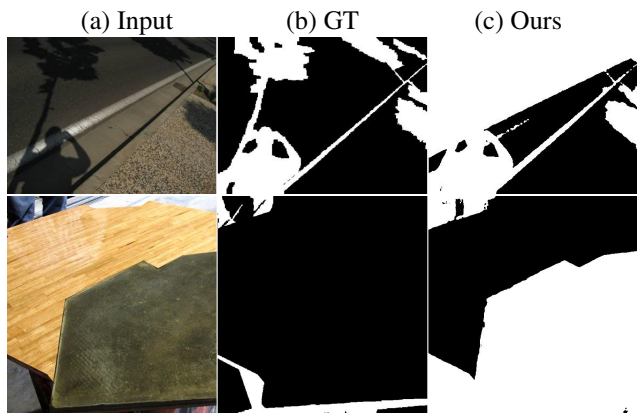


Figure 8: **Failed shadow detection examples.** Failure cases of our method due to non-shadow dark albedo regions. (a) Input image. (b) Ground-truth mask. (c) Predicted shadow mask by our method.

In Figure 7, we show shadow detection results on the SBU dataset. The first, second, and third columns show

the input images, the ground truth shadow masks, and the outputs of D-Net, respectively. We can see how D-Net correctly predicts shadows on different types of scenes such as desert, mountains, snow, and under different climatic conditions from bright sunny to cloudy and overcast days.

We include some failure cases for our method in Figure 8. These are due to dark albedo material regions being incorrectly classified as shadows.

We show additional qualitative results in Figure 9. We can appreciate how D-Net accurately predicts shadows in images depicting close-ups as well as long shots, and aerial images.

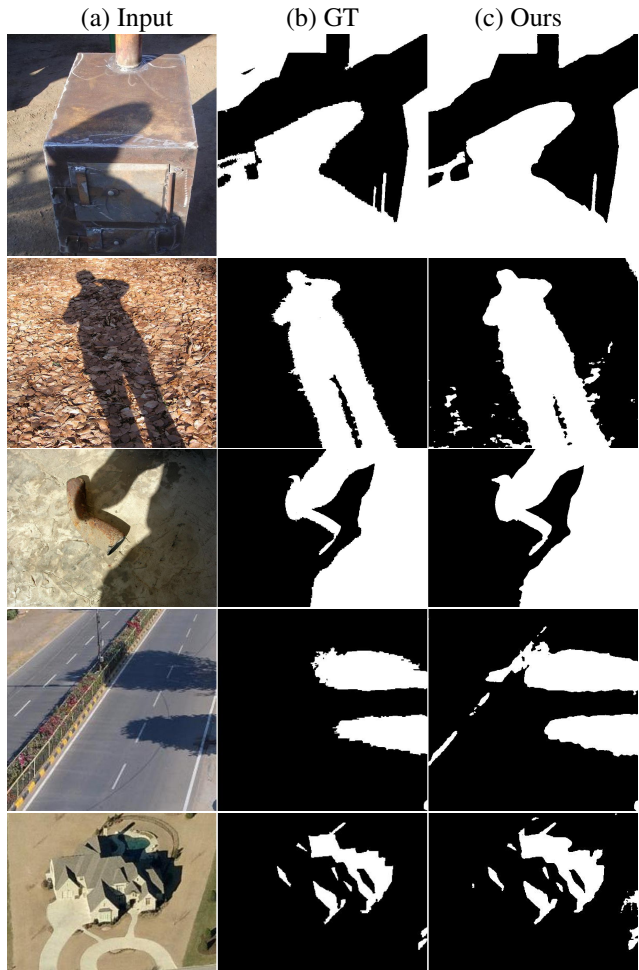


Figure 9: **Shadow detection examples.** Our proposed method accurately detects shadows on close and long shots, as well as aerial images. (a) Input image. (b) Ground-truth shadow mask. (c) Predicted shadow mask by our method.

In Figure 10, we show qualitative comparison with the shadow detection results of scGAN[14]. D-Net predicts overall more accurate shadows with sharper boundaries.

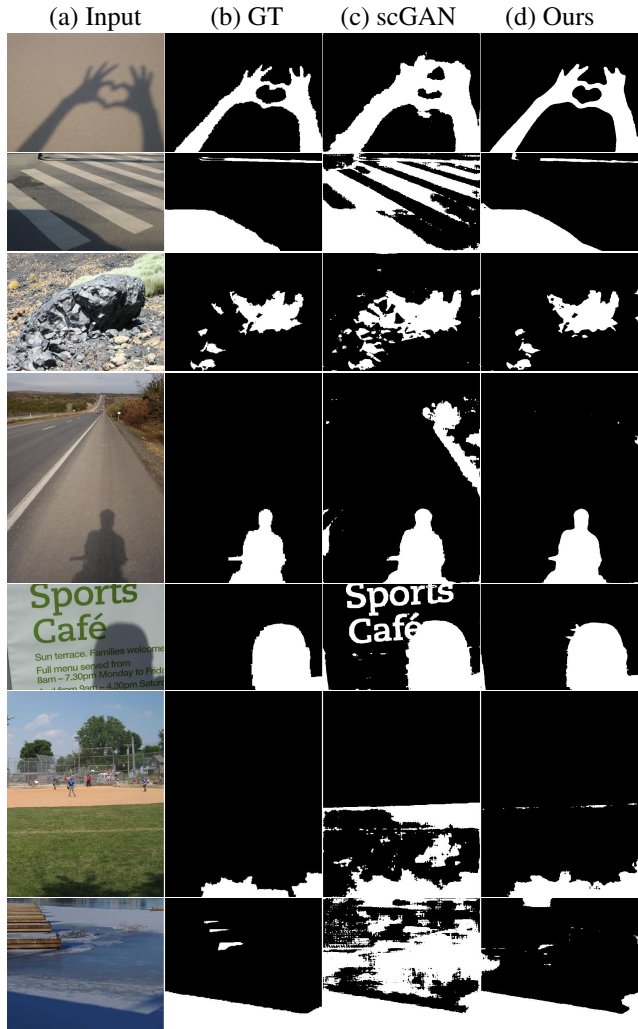


Figure 10: **Comparison of shadow detection on SBU dataset.** Qualitative comparison between our method and the state-of-the-art method scGAN[14]. (a) Input image. (b) Ground-truth shadow mask. (c) Predicted shadow mask by scGAN[14]. (d) Predicted shadow mask by our method.

4.3. Computational Details

We train our model on a single GeForce GTX 1080 Ti GPU. The numbers reported in this paper are results from epoch 50 of our model, which takes approximately 2.5 hours to train on the SBU training dataset.

Table 3 shows the average shadow detection times using the proposed D-Net on SBU testing dataset. We perform experiments resizing the images into 256×256 , 512×512 , and 768×768 before inputting to the network. Image pre-processing (resizing, cropping, normalizing, converting to logarithm) and writing images to disk occupy most of the total detection time. Meanwhile, the prediction time of D-Net is very small and remains almost the same even when

	256×256	512×512	768×768
Image Loading	0.01	0.02	0.02
Pre-Processing	0.02	0.05	0.1
D-Net Prediction	0.01	0.01	0.01
Post-Processing	0.02	0.03	0.06
Image Saving	0.03	0.09	0.19
Total	0.08	0.20	0.38
Frames per second	13	5	3

Table 3: **Average detection times per image.** Average length of detection steps measured in seconds across the whole SBU test set.

the images are 9 times larger (from 256×256 to 768×768). With images resized to 256×256 we can have close-to-real-time shadow detection with 13 frames per second.

4.4. Ablation Study

We conduct the experiment to illustrate the effects of the physics based loss (L_{ph}) on our framework. Table 4 shows the shadow detection results of our model trained with and without the L_{ph} loss. We test our model, trained SBU, on both UCF and SBU testing sets. On the SBU testing set, adding L_{ph} loss brings a 20% improvement to our models performance, in terms of BER reduction. On the cross-dataset task, using L_{ph} also improves overall performance. In this case, our model achieves a 27% error reduction.

Method	Test Set	BER	Shadow	Non Shad.
D-net (A-net with L_{ph})	SBU	5.7	6.2	5.2
D-net (A-net w/o L_{ph})	SBU	7.1	7.6	6.7
D-net (A-net with L_{ph})	UCF	9.9	7.3	12.5
D-net (A-net w/o L_{ph})	UCF	13.6	15.9	11.3

Table 4: **Ablation study.** Comparison of shadow detection results of our framework with and without inclusion of the physics based loss L_{ph} . Detection performance significantly profits from incorporating the physics based loss L_{ph} into the training process: 20% reduction of BER in SBU[22] testing set, and 27% error reduction in UCF[24] (cross-dataset task).

In Figure 11, we compare adversarial examples generated by our model trained with and without the physics based loss L_{ph} . We can see how incorporating L_{ph} produces images with attenuated shadows that look more realistic. Hence, the produced examples aid the training of the shadow detector D-Net.

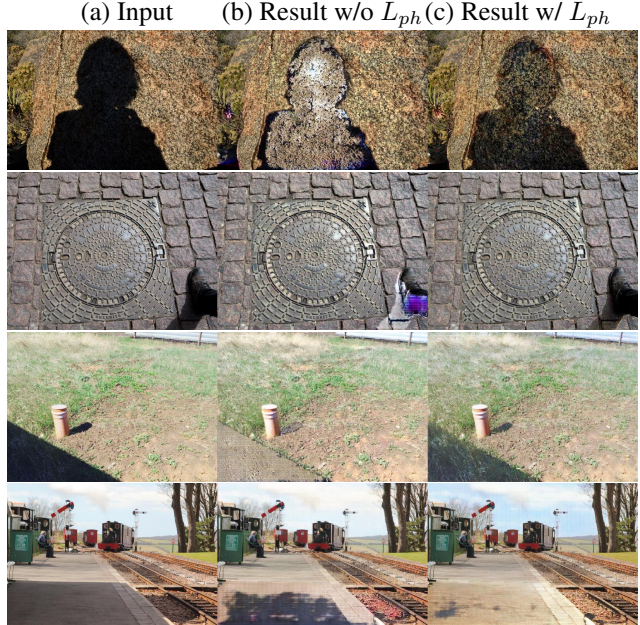


Figure 11: **Examples of adversarial examples generated with and without physics.** (a) Input image I . (b) Adversarial example generated by A-net trained without physics based loss. (c) Adversarial example generated by A-net trained with physics based loss.

5. Summary

In this paper, we have presented a novel framework for adversarial training of a shadow detector using shadow attenuation. We have shown experimentally how our model is able to effectively learn from both real shadow training examples as well as adversarial examples. Our trained model outperforms the previous state-of-art shadow detectors by a wide margin in two benchmark datasets, demonstrating the effectiveness and generalization ability of our model. Furthermore, to the best of our knowledge, this is the first shadow detector that can detect shadows accurately at a speed that is close to real time, 13 fps. This could extend the application of shadow detection to enhance the realism of augmented reality experience.

Acknowledgement. This work was supported by the Vietnam Education Foundation, the Stony Brook University SensorCAT, a gift from Adobe, the Partner University Fund 4DVision project, and the SUNY 2020- Infrastructure, Transportation and Security Center.

References

- [1] G. Finlayson, M. Drew, and C. Lu. Entropy minimization for shadow removal. *International Journal of Computer Vision*, 2009. 1, 2
- [2] G. Finlayson, S. Hordley, C. Lu, and M. Drew. On the re-

- removal of shadows from images. *IEEE Transactions on Pattern Analysis and Machine Intelligence*, 2006. 1, 2
- [3] I. J. Goodfellow, J. Pouget-Abadie, M. Mirza, B. Xu, D. Warde-Farley, S. Ozair, A. C. Courville, and Y. Bengio. Generative adversarial networks. In *Advances in Neural Information Processing Systems*, 2014. 2, 5
- [4] R. Guo, Q. Dai, and D. Hoiem. Single-image shadow detection and removal using paired regions. In *Proceedings of the IEEE Conference on Computer Vision and Pattern Recognition*, 2011. 1, 2, 4
- [5] R. Guo, Q. Dai, and D. Hoiem. Paired regions for shadow detection and removal. *IEEE Transactions on Pattern Analysis and Machine Intelligence*, 2012. 2, 4
- [6] K. He, X. Zhang, S. Ren, and J. Sun. Delving deep into rectifiers: Surpassing human-level performance on imagenet classification. In *Proceedings of the 2015 IEEE International Conference on Computer Vision (ICCV)*, ICCV '15, pages 1026–1034, Washington, DC, USA, 2015. IEEE Computer Society. 4
- [7] X. Huang, G. Hua, J. Tumblin, and L. Williams. What characterizes a shadow boundary under the sun and sky? In *Proceedings of the International Conference on Computer Vision*, 2011. 2
- [8] P. Isola, J.-Y. Zhu, T. Zhou, and A. A. Efros. Image-to-image translation with conditional adversarial networks. *arxiv*, 2016. 4
- [9] H. Khan, M. Bennamoun, F. Sohel, and R. Togneri. Automatic feature learning for robust shadow detection. In *Proceedings of the IEEE Conference on Computer Vision and Pattern Recognition*, 2014. 1, 2
- [10] D. P. Kingma and J. Ba. Adam: A method for stochastic optimization. *CoRR*, abs/1412.6980, 2014. 5
- [11] J.-F. Lalonde, A. A. Efros, and S. G. Narasimhan. Detecting ground shadows in outdoor consumer photographs. In *Proceedings of the European Conference on Computer Vision*, 2010. 1, 2
- [12] M. Mirza and S. Osindero. Conditional generative adversarial nets. *arXiv preprint arXiv:1411.1784*, 2014. 2
- [13] S.-M. Moosavi-Dezfooli, A. Fawzi, O. Fawzi, and P. Frossard. Universal adversarial perturbations. In *Proceedings of the IEEE Conference on Computer Vision and Pattern Recognition*, July 2017. 3
- [14] V. Nguyen, T. F. Y. Vicente, M. Zhao, M. Hoai, and D. Samaras. Shadow detection with conditional generative adversarial networks. In *Proceedings of the International Conference on Computer Vision*, 2017. 1, 2, 6, 7
- [15] A. Panagopoulos, C. Wang, D. Samaras, and N. Paragios. Simultaneous cast shadows, illumination and geometry inference using hypergraphs. *IEEE Transactions on Pattern Analysis and Machine Intelligence*, 2013. 1
- [16] L. Qu, J. Tian, S. He, Y. Tang, and R. W. H. Lau. Dshadownet: A multi-context embedding deep network for shadow removal. In *Proceedings of the IEEE Conference on Computer Vision and Pattern Recognition*, July 2017. 2
- [17] O. Ronneberger, P. Fischer, and T. Brox. U-net: Convolutional networks for biomedical image segmentation. In *Medical Image Computing and Computer-Assisted Intervention (MICCAI)*, volume 9351 of LNCS, pages 234–241. Springer, 2015. (available on arXiv:1505.04597 [cs.CV]). 4
- [18] A. Shrivastava, T. Pfister, O. Tuzel, J. Susskind, W. Wang, and R. Webb. Learning from simulated and unsupervised images through adversarial training. In *Proceedings of the IEEE Conference on Computer Vision and Pattern Recognition*, 2016. 2, 3
- [19] K. Sunkavalli, W. Matusik, H. Pfister, and S. Rusinkiewicz. Factored time-lapse video. *ACM Transactions on Graphics (Proc. SIGGRAPH)*, 26(3), August 2007. 1
- [20] T. F. Y. Vicente, M. Hoai, and D. Samaras. Leave-one-out kernel optimization for shadow detection. In *Proceedings of the International Conference on Computer Vision*, 2015. 1, 2
- [21] T. F. Y. Vicente, M. Hoai, and D. Samaras. Noisy label recovery for shadow detection in unfamiliar domains. In *Proceedings of the IEEE Conference on Computer Vision and Pattern Recognition*, 2016. 2
- [22] T. F. Y. Vicente, L. Hou, C.-P. Yu, M. Hoai, and D. Samaras. Large-scale training of shadow detectors with noisily-annotated shadow examples. In *Proceedings of the European Conference on Computer Vision*, 2016. 1, 2, 5, 6, 8
- [23] S. Wehrwein, K. Bala, and N. Snavely. Shadow detection and sun direction in photo collections. In *Proceedings of 3DV*, 2015. 1
- [24] J. Zhu, K. Samuel, S. Masood, and M. Tappen. Learning to recognize shadows in monochromatic natural images. In *Proceedings of the IEEE Conference on Computer Vision and Pattern Recognition*, 2010. 1, 2, 5, 6, 8